Universiteit Antwerpen

This item is the archived peer-reviewed author-version of:

Influence of neutron irradiation on X-ray diffraction, Raman spectrum and photoluminescence from pyrolytic and hot-pressed hexagonal boron nitride

uantwerpen.be

Institutional repository IRUA

Influence of neutron irradiation on X-ray diffraction, Raman spectrum and photoluminescence from pyrolytic and hot-pressed hexagonal boron nitride

Shun Zhou [1], Wen Xu [1, 2, 3, *], Yiming Xiao [1, †], Huan Xiao [1], Jing Zhang [2], Zhu Wang [4, 5, ‡], Gaokui He [6], Jing Liu [7], Yuanyuan Li [7], and François M. Peeters [3, 8]

[1]School of Physics and Astronomy and Yunnan Key Laboratory for Quantum Information, Yunnan University, Kunming 650504, China

[2]Key Laboratory of Materials Physics, Institute of Solid State Physics, Chinese Academy of Sciences, Hefei 230031, China

[3]Micro Optical Instruments Inc., Shenzhen 518118, China

[4]Hubei Key Laboratory of Radiation Chemistry and Functional Materials, School of Nuclear Technology, Chemistry and Biology, Hubei University of Science and Technology, Xianning 437100, China

[5]Key Lab of Artificial Micro- and Nano-Structures of Ministry of Education of China, School of Physics and Technology, Wuhan University, Wuhan 430072, China

[6]China Institute of Atomic Energy, Beijing 102413, China

[7]The State Key Laboratory of Refractories and Metallurgy, Wuhan University of Science and Technology, Wuhan, Hubei 430081, China

[8]Department of Physics, University of Antwerp, Groenenborgerlaan 171, B-2020 Antwerp, Belgium

∗ Electronic address: wenxu_issp@aliyun.com

† Electronic address: yiming.xiao@foxmail.com

‡ Electronic address: wangz@whu.edu.cn

Abstract: Hexagonal boron nitride (hBN) is considered as an ideal semiconductor material for solid-state neutron detector, owing to its large neutron scattering section because of the low atomic number of B and excellent physical properties. Here we study the influence of neutron irradiation on crystal structure and on intermediate energy state (IMES) levels induced by the presence of impurities and defects in hBN. Large-size and thick pyrolytic and hot-pressed hBN (PBN and HBN) samples, which can be directly applied for neutron detector devices, are prepared and bombarded by neutrons with different irradiation fluences. The SEM and TEM are used to observe the sample difference of PBN and HBN. X-ray diffraction and Raman spectroscopy are applied to examine the influence of neutron irradiation on lattice structures along different crystal directions of PBN and HBN samples. Photoluminescence (PL) is employed to study the effect of neutron irradiation on IMESs in these samples. We find that the neutron irradiation does not alter the in-plane lattice structures of both PBN and HBN samples, but it can release the inter-layer tensions induced by sample growth of the PBN samples. Interestingly and surprisingly, the neutron irradiation does not affect the IMES levels responsible for PL generation, where PL is attributed mainly from phonon-assisted radiative electron-hole coupling for both PBN and HBN samples. Furthermore, the results indicate that the neutron irradiation can weaken the effective carrier-phonon coupling and exciton transitions in PBN and HBN samples. Overall, both PBN and HBN samples show some degree of the resistance to neutron irradiation in terms of these basic physical properties. The interesting and important findings from this work can help us to gain an in-depth understanding of the influence of neutron irradiation on basic physical properties of hBN materials. These effects can be taken into account when designing and applying the hBN materials for neutron detectors.

Keywords: hexagonal boron nitride, neutron irradiation, X-ray diffraction, Raman spectrum, Photoluminescence

1. Introduction

With the development of nuclear industry and the application of nuclear science and technology, there has been a huge and urgent demand for developing the cheap, compact, light weight, environmental friendly, and high sensitive neutron detectors to at least partly replace He-based gas neutron detectors [1, 2] and to explore the new applications of nuclear technologies [3, 4]. Solid state neutron detector is one of the most practical options to meet these requirements. Due to the low atomic numbers of B and N, boron nitride (BN) has a large neutron scattering section and insensitive to γ-ray. Therefore, it has been considered as neutron detecting material. BN is a white and crystalline semiconductor, commonly with a hexagonal lattice structure similar to that of graphite [5]. Hexagonal BN (hBN) has already emerged as a realm of great interest for advanced electronic and optoelectronic devices, because of its distinguishable characteristics such as high chemical and thermal stability [6], strong mechanical strength [7], low dielectric constant [8], low leakage current [6], near-zero polarization [9], very wide band gap [6], resistant to oxidation and nuclear radiation [10, 11], etc. These features make hBN further important and unique for neutron detector based on state-of-the-art electronic technology. At present, hBN based neutron detector has been preliminarily realized and its excellent ability for neutron detection has been experimentally demonstrated [12, 13]. However, because currently it is very difficult and expensive to obtain large-size and thick high quality single crystal hBN, poly-crystalline hBN materials are often used for testing and studying the neutron detection [14]. In the synthesis and growth of these poly-crystal hBN, it is inevitable to introduce the impurities and defects in the hBN samples. The crystal and sample structures, along with the impurities and defects in hBN materials prepared by different techniques, can expectedly affect the performance of hBN based neutron detectors. Therefore, it is of great importance and significance to examine the influence of neutron irradiation on crystal and sample structures and on impurities and defects in hBN materials. This becomes the prime motivation of the present study.

From a viewpoint of physics, hBN is a conventional semiconductor, where B is sandwiched between two N layers. Therefore, hBN is basically a layered semiconductor and its crystal is consist of hBN layers with van der Waals type of inter-layer bonding [15]. Its basic physical and chemical properties have been relatively well known [16]. However, the influence of neutron irradiation on these properties is still a topic of research. Up to the present, the experimental research on the effect

of neutron irradiation on hBN materials has been conducted for the neutron damage [17], structural defects [18, 19], swelling [20], thermal neutron shielding [21], color centers [22], etc. In particular, the effect of neutron irradiation on [10]B- and [11]B-enriched hBN crystal flakes has been studied very recently [18] by using different measurement techniques. The results demonstrate that the point defects in hBN can play an important role in affacting the electronic and optical properties of hBN after neutron irradiation and, thus, the defect engineering of hBN via neutron transmutation doping has been proposed [18]. In this work, we prepare two types of large-size and thick hBN samples using pyrolytic and hot-press techniques [23] respectively. The SEM and TEM are used to observe the basic difference of these two types of hBN samples. Because the strongest characteristic X-ray diffraction (XRD) peak comes from (002)-plane of hBN [24], we apply the XRD to examine the influence of neutron irradiation on crystal and sample structure along the c-axis or growth-direction of hBN samples. On the basis that the characteristic Raman mode E_{2g} is induced by in-plane lattice vibrations in hBN [25], we employ the Raman spectroscopy to study the influence of neutron irradiation on crystal and sample structure, along with carrier-phonon coupling, in the xy-plane or in-plane directions of the hBN samples. Furthermore, owing to the fact that the photoluminescence (PL) can be measured in visible bandwidth when excitation photon energy is less than the band gap of hBN [26], we apply the PL to investigate the influence of neutron irradiation on intermediate energy levels induced by the presence of impurities and defects in hBN materials. Our aim of these studies is at examining how neutron irradiation can affect the basic physical properties of hBN materials fabricated by two different techniques. The results obtained from these studies can be taken into consideration when designing and applying the hBN materials for neutron detection.

2. Samples preparation and SAM and TEM images

In applying hBN materials for neutron detection, large-size sample with relatively thick thickness is necessarily required because the neutron scattering section increases exponentially with the sample thickness [27]. At present, it is very difficult and very expensive to obtain the large-size and thick single crystal hBN [28]. Pyrolytic and hot-press techniques are often applied to grow the large-size hBN samples consisting normally of the poly-crystalline structures. In this study, we prepared two types of hBN samples which can be directly applied for the realization of neutron detectors. The pyrolytic hBN (PBN) sample was produced by using the standard high-temperature chemical

vapor deposition (CVD) [29]. The depositions were achieved under low pressure in a vertical hot-wall CVD system, where borazine was used as single source B precursor and nitrogen was used as carrier and dilute gas. The samples were grown in the temperature range from 1300 ℃ to 1600 ℃, with a total pressure of 200 Pa. Prior to the deposition, the graphite substrates were polished with grinder and ultrasonically cleaned respectively in acetone and distilled water. The as-deposited PBN sample can be peeled off from the substrate automatically during the cooling step of the reactor. The hot pressed hBN (HBN) sample was fabricated by applying the standard hot-press technique [30], where the reactive hot-pressing on a graphite die with BN coating was achieved at 1900 ℃ under a pressure of 50 MPa for 60 minutes. In using this technique, B_2O_3 was taken as sintering additive in a nitrogen atmosphere. The as-grown PBN and HBN wafers were cut into smaller pieces as samples respectively and each sample is about 14 mm×14 mm in area and 1 mm thick along the growth direction. These samples were cleaned in acetone or ethanol, followed by a deionized water bath. Before neutron irradiation, these samples look white and opaque to the daylight.
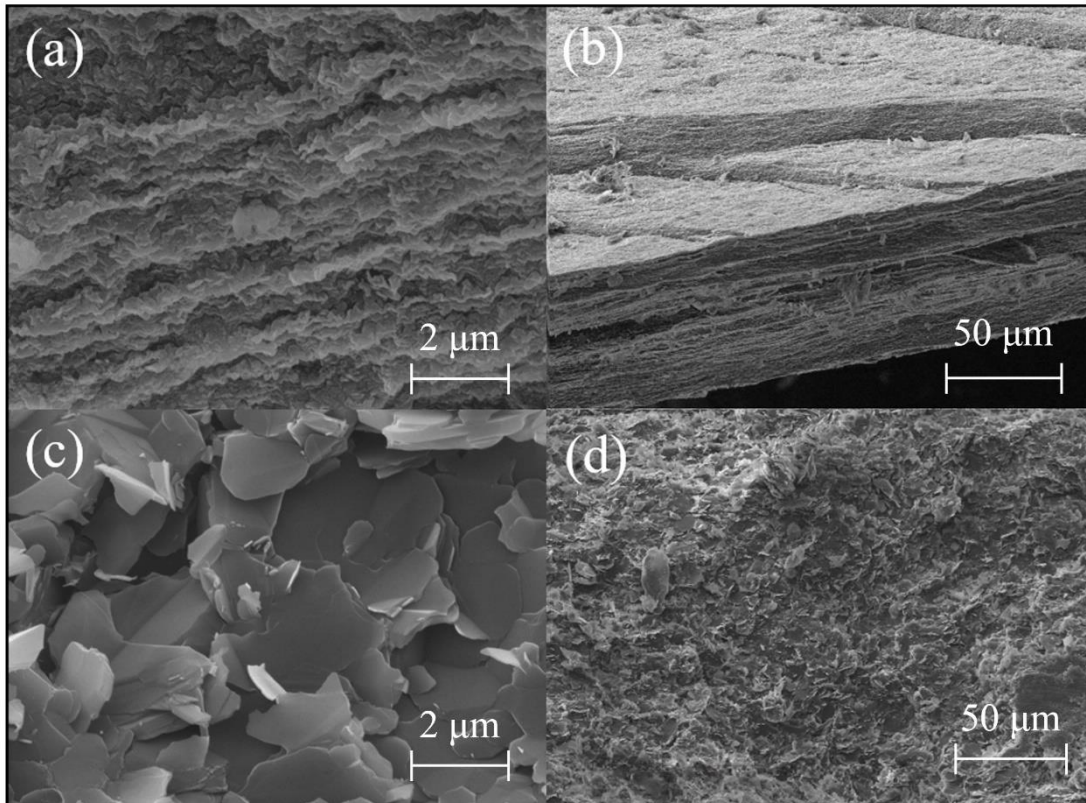

Fig. 1: SEM images of PBN [(a) and (b)] and HBN [(c) and (d)] samples before neutron irradiation with different magnifications as indicated.
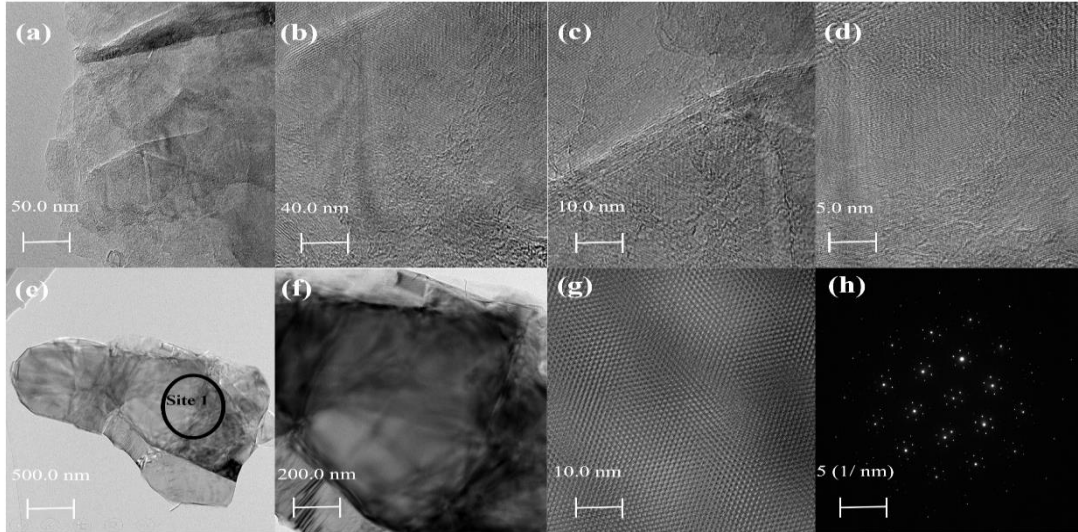
Fig. 2: TEM images of PBN and HBN samples before neutron irradiation. Here, (a)-(d) are images of PBN sample with different magnifications, (e) is the image of HBN sample with a magnification of 500 nm, (f) and (g) show the locally amplifed images of (e), and (h) shows the SAED patter of HBN sample before neutron irradiation.

To observe one of the the basic differences of our PBN and HBN samples before neutron irradiation, in Fig. 1 and Fig. 2 we show respectively the SEM and TEM images of them. From Fig. 1 we see that the PBN sample grown by CVD is composed by thin hBN films and these thin films are stacked to form the layered structure along the z- or growth-direction as shown in Fig. 1 (a) and (b). In contrast, the HBN sample is consist of micron-sized (about 2-3 μm) hBN thin flakes and these flakes are randomly distributed along all directions (as shown in Fig. 1 (c) and (d)). Thus, HBN sample is without the layered sample structure as PBN is, although the hBN itself is with a layered crystal structure. To take the TEM images, we grinded the PBN and HBN samples into powders respectively, dispersed them uniformly in alcohol and evenly dropped them onto a copper mesh. From TEM images of PBN sample shown in Fig. 2 (a) - (d), we see that: i) a hBN thin film is composed by thin hBN crystals with the size about 50 nm and the random shapes (Fig. 2(a)); ii) the folds can be found in these thin hBN crystals (Fig. (2b)); iii) these thin hBN crystals are stacked or in the form of poly-crystals (Fig. 2(c)) to form the thin hBN films; and iv) the good hBN crystal structure can be observed in at least 5-10 nm scale (Fig. 2(d)). Fig 2(e) is the TEM image of HBN sample before neutron irradiation with a magnification of 500 nm, while Fig. 2(f) and (g) show the

local amplifications of site 1 indicated in Fig. 2(e). We can see that the HBN sample shows the different images compared to those for PBN sample. Because the hBN thin flakes in HBN are randomly distributed along the growth-direction, the image with 200 nm magnification cannot be clearly taken (see Fig. 2(f)). However, the lattice image for HPN sample (Fig. 2(g)) is much better than that for PBN sample (Fig. 2(c)) with 10 nm magnification and the folds are not found in HBN sample in this regime. Therefore, HBN sample is with a better crystal quality than PBN sample. Fig. 2(h) shows the SAED pattern of the HBN sample. We can see very symmetric and identical hexagonal patterns in the measured area, indicating that the hBN lattice in HBN sample is not deformed due to the random distribution of the thin hBN flakes. From a viewpoint of material physics, two different formations of hBN poly-crystalline structures in PBN and HBN samples can result in, at least, different stresses and strains along the z- or growth-direction of the hBN samples. This may become a basis on the understanding of some results obtained from this study.

3. Neutron irradiation

Table I: The NIFs on hBN samples.

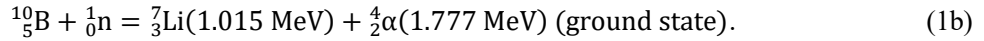| Sample	Sample No.	Fluence /$n \cdot cm^{-2}$
PBN	A1	0
	A2	3.91×10^{14}
	A3	1.57×10^{15}
	A4	1.00×10^{16}
HBN	B1	0
	B2	3.98×10^{14}
	B3	1.98×10^{15}
	B4	1.00×10^{16}

The PBN and HBN samples prepared in this work were bombarded by neutrons with different irradiation fluences. The experiments were conducted at the Research Nuclear Reactor Facility in

China Institute of atomic Energy. For convenience, we name the PBN and HBN samples as group A and group B respectively. In neutron irradiation experiment, the sample was placed inside sealed polyethylene flasks (1.5 cm in diameter and 4.5 cm in height) and irradiated inside the reactor with an neutron flux of $I = 5 \times 10^{11} \, n \cdot cm^{-2} \, s^{-1}$, where n is the neutron number. The neutron irradiation fluence (NIF) on a sample is evaluated by $I \times t$ with t being the irradiation time. In Table I, we show the NIF on different samples.

We find that with increasing NIF, the colors of both PBN and HBN samples turn from white (A1 and B1) to light-red (A2 and B2), red (A3 and B3) and dark-red (A4 and B4). This is the consequence of the production of Li by neutron irradiation on hBN [18] through the reactions [20]:

$$^{10}_{5}B + ^{1}_{0}n = ^{7}_{3}Li^{*}(0.84 \text{ MeV}) + ^{4}_{2}\alpha^{*}(1.47 \text{ MeV}) \text{ (excited state)}, \tag{1a}$$

and

$$^{10}_{5}B + ^{1}_{0}n = ^{7}_{3}Li(1.015 \text{ MeV}) + ^{4}_{2}\alpha(1.777 \text{ MeV}) \text{ (ground state)}. \tag{1b}$$
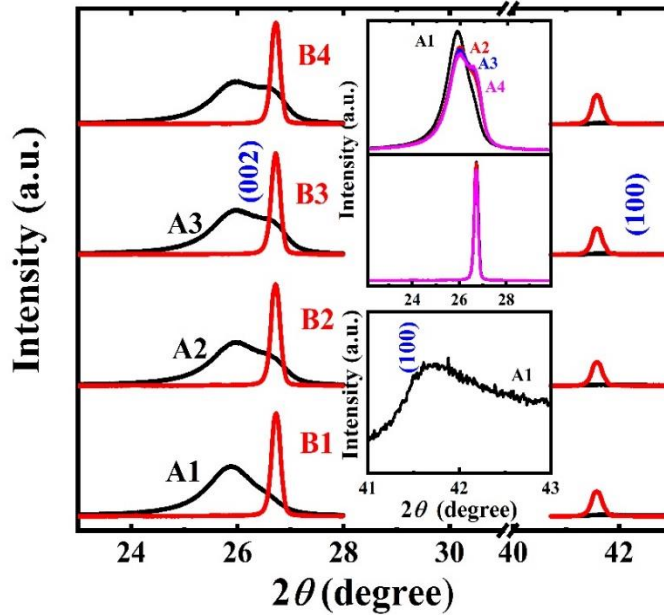
4. X-ray diffraction

Fig. 3 XRD spectra of PBN (A1-A4) and HBN (B1-B4) samples under different neutron irradiation fluences (see Table I). The insets show the effect of neutron irradiation on (002) XRD peak for PBN (upper pannel) and HBN (middle panel, where four curves for B1-B4 coincide roughly) samples, along with the weak (100) XRD peak for A1 (lower panel).

In this study, we apply the XRD to examine the influence of neutron irradiation on crystal properties of PBN and HBN samples and the results are shown in Fig. 3. Before neutron irradiation (A1 and B1 samples), we can observe the sharp characteristic XRD peaks for B1 sample, which are located at about 26.7° for diffraction from (002)-plane and at about 41.5° from (100)-plane. For A1, we can clearly measure one XRD peak located at about 25.9°, shifting from the characteristic peak at 26.7°. This peak looks broadened and obviously lower than that for B1. A very weak XRD peak from (100)-plane diffraction can be observed at about 41.7 ° for A1 sample (see lower pannel in inset). It is known that the strongest characteristic XRD peak for hBN is induced by diffraction from (002)-plane [24], namely the lattice constant along the c-axis or out-plane direction of hBN crystal determines mainly the position of the XRD peak from (002)-plane. Because PBN sample is formed by layered structure (see Fig. 1(b)), the inter-layer stress induced by sample growth can result in strains on hBN crystals in the thin films and, thus, alter the lattice constant along the c-axis of hBN. Consequently, the shift of the XRD peak can be observed. The results shown in Fig. 3 suggest that the inter-layer stress in PBN samples is tension-like, which can lead to a larger lattice constant along the c-axis and, therefore, a smaller diffraction angle for (002)-plane because a smaller XRD angle corresponds a larger lattice constant [31]. Because the hBN grain size in HBN sample (B1) is much larger than that in PBN sample (A1), a stronger XRD peak is expected to be observed for HBN sample. From Fig. 3, we find that these basic features do not change significantly after neutron irradiation with different fluences. However, it is interesting to notice that after neutron irradiation, the XRD peak for PBN samples (A2-A4) can be decomposed into two peaks, one located at 26.7° and another at 25.9°, and the component from 26.7° diffraction increases with NIF. This finding implies that the neutron irradiation can release and easy the inter-layer tensions in PBN samples. In the inset of Fig. 3, we show the effect of neutron irradiation on (002) XRD peaks for PBN (upper panel) and HBN (middle panel) samples. It shows that with increasing NIF, the peak height for PBN sample lowers but the peak looks more broadened, whereas the height and width of the XRD peak for HBN samples do not change markedly. These results indicate that the neutron irradiation affects very weakly the hBN lattice structure of HBN sample but can release the inter-layer tensions for layered PBN sample grown by CVD technique. Namely, HBN samples can have stronger resistance to neutron irradiation along the c-axis or sample growth-direction than PBN samples.
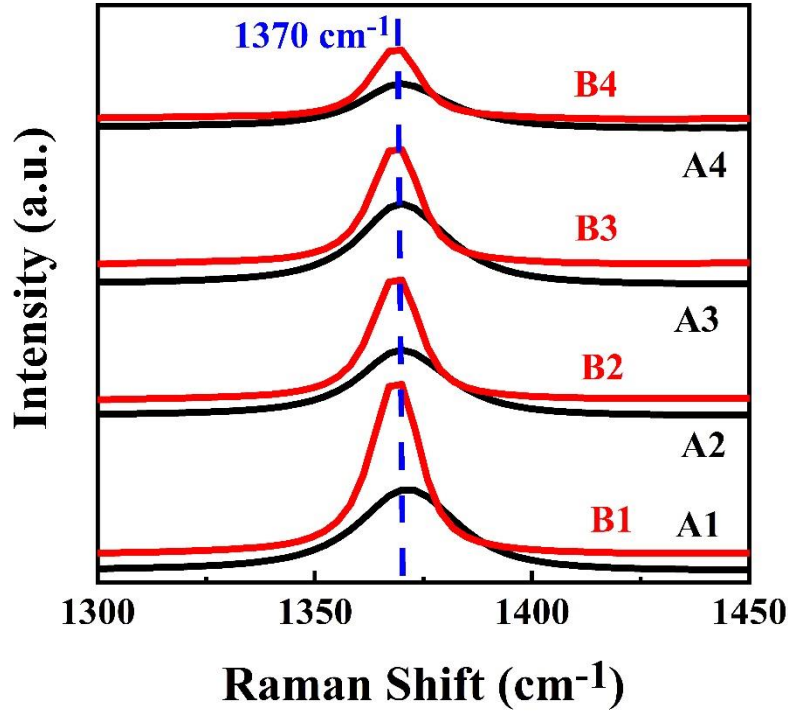
9

5. Raman Spectroscopy

Fig 4: Raman spectra for PBN (black curves) and HBN (red curves) samples with different neutron irradiation fluences (see Table I). The excitation laser wavelength is 785 nm and the measurements were conducted at room temperature.

We measure the Raman spectra for PBN and HBN samples before and after neutron irradiation, where a 785 nm wavelength laser was applied for excitation and the measurements were carried out at room temperature. The usage of relatively long wavelength laser excitation here can greatly reduce the PL signals from hBN samples and can obtain the clear Raman signals. The corresponding results are presented in Fig. 4. The following features can be noticed. i) The positions of Raman peaks for PBN and HBN samples are basically the same, which is located at about 1370 cm^{-1}. This peak corresponds to the characteristic Raman mode E_{2g} induced by in-plane lattice vibrations in hBN [25] and to a longitudinal-optical (LO) phonon energy of 171 meV [32]. We can believe that the in-plane crystal structures in PBN and HBN samples are roughly the same because this is the in-plane Raman mode. This result confirms further that the PBN and HBN samples prepared in this work are actually with the hexagonal BN crystal structure. ii) The Raman peaks for HBN samples are obviously higher than those for PBN samples. This implies that the photon-excited carrier-

10

phonon coupling in HBN samples is stronger than that in PBN samples. This is because of the larger hBN grain size in HBN samples than that in PBN samples. iii) Compared to PBN samples, the Raman lines for HBN samples are narrower because HBN samples are with better crystal quality [18]. And iv) with increasing NIF, the positions of the Raman peaks for PBN and HBN samples do not shift and the height of the peak decreases markedly. This indicates that the neutron irradiation does not alter the basic in-plane crystal structures and the LO-phonon modes in both PBN and HBN samples and, however, it can weaken the effective carrier-phonon coupling in hBN samples, in consistent with that obtained from our terahertz time-domain spectroscopy (THz TDS) measurements [33]. The main physical reason behind this effect is that the neutron irradiation can induce the defects and carrier trap centers in hBN [18, 34], which can reduce the conducting carrier density and reduce the effective carrier-phonon interaction.
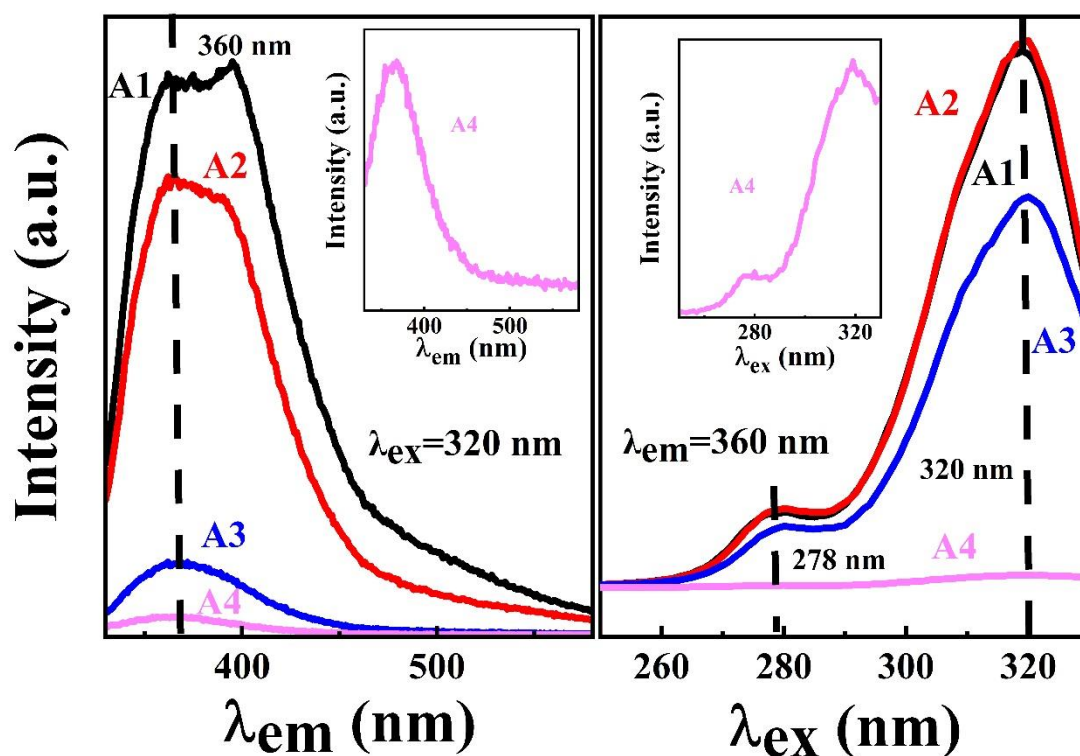
6. Photoluminescence

Fig. 5: Left panel: PL spectra from PBN samples with different NIFs (see Table I), excited by λ_{ex} = 320 nm wavelength light. Right panel: PLE spectra from PBN samples measured at a fixed emission wavelength λ_{em} = 360 nm. The insets show the corresponding results for A4 in different PL intensity scales.

We apply the photoluminescence (PL) to study the effect of neutron irradiation on opto-electronic properties of PBN and HBN samples. It is known that the energy-gap between the conduction- and valence-band in hBN is about 6.1 eV. During the growth of hBN samples, the impurities (e.g., H- and O-based chemical bonds and functional groups) and defects (e.g, N- and B-vacancies) can be introduced [35]. Similar to conventional semiconductors, the presence of these impurities and defects in hBN can form the intermediate energy state (IMES) levels in-between the conduction and valence bands. As a result, the PL emission can be observed in hBN when excitation photon energy is less than the band-gap of hBN [36]. In this study, we take the xenon lamp as the excitation light source to measure the PL from hBN samples, where the measurements were undertaken at room temperature. The advantage to apply xenon lamp as excitation light is that we can measure the PL intensity at a fixed emission wavelength as a function of excitation wavelength, namely we are able to measure the PL emission (PLE) spectrum.
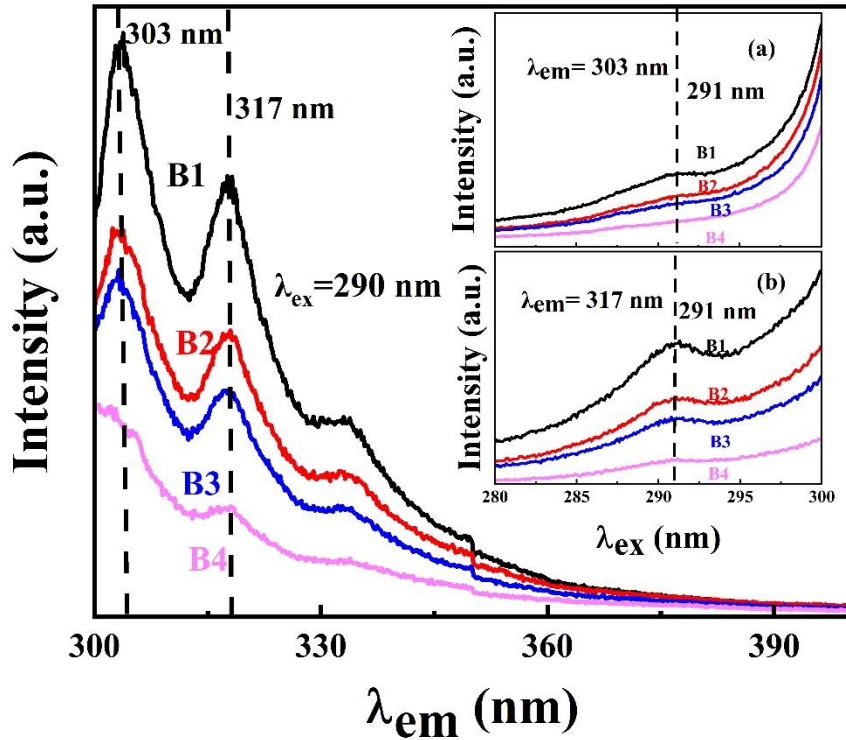

Fig. 6: PL spectra from HBN samples with different NIFs (see Table I), excited by λ_{ex} = 290 nm wavelength light. The inset shows the PLE spectra for B1-B4 samples measured at the fixed emission wavelength λ_{em} =303 nm (upper panel) and λ_{em} =317 nm (lower panel).

12

In the left panel of Fig. 5, we show the PL spectra from PBN samples excited by a fixed light wavelength λ_{ex} = 320 nm. Before neutron irradiation, A1 sample exhibits a rather broad PL peak shape at about 360 nm and, with increasing NIF, this broad peak becomes sharper (see inset). We find that the PL spectra for PBN samples can be decomposed into two peaks, one is at about 361 nm and another is at about 383 nm, via Gaussian fitting. The results of the decompositions are presented in the Supplementary Materials. We note that the energy difference between these two peaks is about 196 meV, quite close to LO-phonon energy of hBN crystal. Our Raman results shown in Fig. 4 suggest that the LO-phonon energy in our PBN and HBN samples is about 171 meV. From the insets in Fig. S1 in Supplementary Materials, it can be seen that the amplitudes of the decompsed two peaks decrease with increasing NIF. In Fig. 6, we show the PL spectra from HBN samples excited by a fixed light wavelength λ_{ex} = 290 nm. In sharp contrast to PBN samples, two sharp PL peaks can be observed for HBN samples, one is located at about λ_{em} =303 nm and another is at about 317 nm. The energy difference between these two peaks is about 175 meV, very close to the LO-phonon energy in hBN. The amplidutes of these two peaks also decrease with increasing NIF.

The PLE spectra for PBN samples are shwon in the right panel in Fig. 5, measured at a fixed PL emission wavelength λ_{em} = 360 nm. We notice that there are two PLE peaks located at about 278 nm and 320 nm respectively, suggesting that there are two active IMES levels responsible for the PL observed at 360 nm for PBN samples. In the insets in Fig. 6, the PLE spectra measured at the fixed λ_{em} =303 nm (upper panel) and at λ_{em} =317 nm (lower panel) are presented for HBN samples. Interestingly and surprisingly, only one PLE peak located at about 291 nm can be found for both λ_{em} =303 nm and 317 nm, implying that there is only one active IMES level responsible for two PL peaks at 303 nm and 317 nm.

From Fig. 5 and Fig. 6 we note that the neutron irradiation does not alter, roughly speaking, the PL peak positions around 360 nm for PBN samples and around 303 nm and 317 nm for HBN samples, suggesting that the neutron irradiation does not affect the IMES levels induced by impurities and defects and responsible for the PL processes. Moreover, the neutron irradiation can obviously lower the intensities of PL and PLE for both PBN and HBN samples, implying that the irradiation can weaken the excitonic or radiative electronic transitions among the active IMES levels in hBN materials.

7. Further discussions

Here we discuss the results obtained from PL measurements on our PBN and HBN samples. hBN is an indirect gap semiconductor with fundamental indirect excitons or electron-hole pairs lying in-between the conduction and valence bands [37]. When excitation photon energy is less than the energy gap, the excitonic transitions accompanied by the emision of photons in hBN are mainly achieved via electronic transitions among the IMESs induced by the presence of impurities and defects. These electronic transitions have to obye the momentun and energy conservation laws. Hence, the radiative recombination of electron-hole pairs must involve coupling with phonons in hBN [37]. In the UV regime where the emitted photon energies are in-between 5.0-6.0 eV, the PL signals corresponding to phonon-assisted emission in hBN have been observed [37] and the influence of neutron irradiation on these emission processes have been discussed [18]. The results shown in Fig. 5 and Fig. S1 for PBN samples and in Fig. 6 for HBN samples suggest that the PL generation from hBN in visible regime is also induced by phonon-assisted excitonic transitions, evident by the fact that the energy spacing between two PL peaks is close to the LO-phonon energy in PBN and HBN samples. Because the phonon modes and the strength of carrier-phonon coupling depend strongly on the crystallinity of an electronic material, the intensity, line-shape and the PL peak position rely also on the crystal quality of hBN [18, 37]. The results obtained from our SEM, TEM, XRD and Raman measurements indicate that our HBN sample is with the better hBN crystallinity than PBN sample is. This is the main reason why the sharper PL peaks can be observed in HBN samples than those in PBN samples.

As has been pointed out [18,34], the neutron irradiation can induce the defects and carrier trap centers in hBN [18, 34]. It is known that the defects induced by neutron irradiation are evenly distributed in the sample without introducing impurity-like ions [38]. However, these defects can play the roles as carrier trapping centers. The induced defects can be destructive to crystallinity of the hBN crystal and, thus, weaken the phonon modes. The presence of the carrier trap centers can reduce the conducting carrier density. These factors can significantly weaken the effective carrier-phonon interactions and, therefore, reduce the possibility for excitonic or radiative electronic transitions among the active IMES levels in hBN materials. As a result, the intensities of PL and PLE for both PBN and HBN samples decrease with increasing NIF, as shown in Fig. 5, Fig. S1 and Fig. 6. This reduced PL intensity by neutron irradiation has also been observed for ^{10}B- and ^{11}B-

enriched hBN crystal flakes [18]. Moreover, from the results shown in Fig. S1, we see that the lower frequency PL peaks centered at about 383 nm for HBN samples decay rapidly with increasing NIF. This is a main reason why the PL peaks in Fig. 5 become sharper with the increase of NIF.
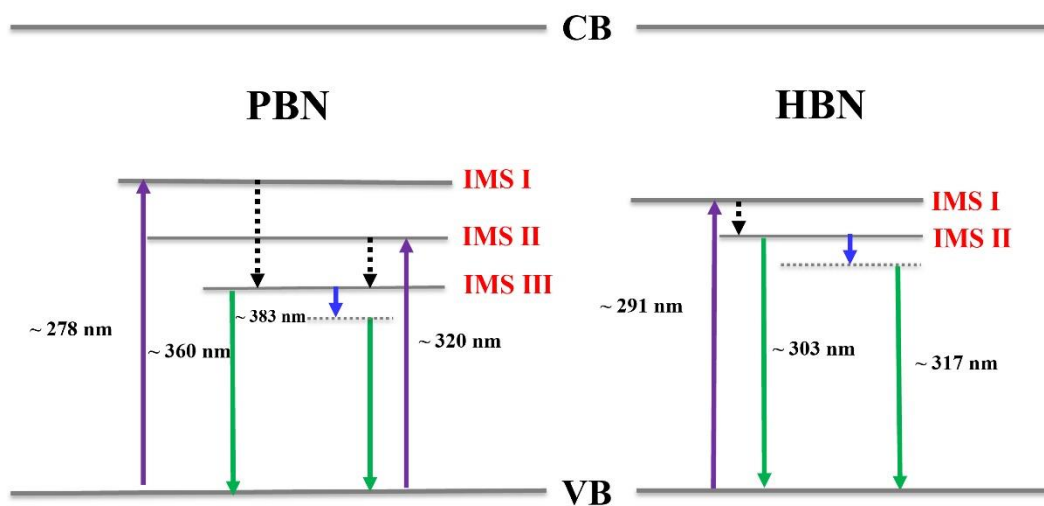

Fig. 7: Energy diagram illustrating the PL processes in PBN and HBN samples. Here, IMS stands for intermediate states induced by the presence of impurities and defects in the sample, the purple lines refer to optical excitations (determined by PLE spectra), the dotted thick vertical lines are for nonradiative electronic transitions and the green lines are PL emission chanels (peak positions in PL spectra), the dotted thin parallel lines are phonon-assisted emission levels, and the bule arrows stand for phonon emission transitions.

From the results shown in Fig. 5, Fig. S1 and Fig. 6, we can figure out that the active energy levels responsible for PL generation from PBN and HBN samples when excitation photon energy is less than the band gap of hBN, as shown in Fig. 7. In this study, we find that two PL peaks can be observed in 290 nm – 500 nm wavelength regime for PBN and HBN samples, although the two peaks in PBN sample can only be seen via decomposision. The energy difference between these two PL peaks is close to the LO-phonon energy of hBN. Thus, we may propose a possible mechanism for PL generation from hBN materials when excitation photon energy is less than the band gap of hBN. Under the action of excitation photons, the electrons in the valence band in hBN are excited

into the IMESs (the purple lines in Fig. 7) which are located in-between the conduction and valence bands. The electron-hole pairs then can be formed similar to excitons. The excited electrons in the higher IMES levels (IMS I and IMS II for PBN and IMS I for HBN in Fig. 7) can relax into the lower IMES levels (IMS III for PBN and IMS II for HBN in Fig. 7) via non-radiative electronic transitions mediated by phonon scattering (the dotted thick vertical lines in Fig. 7). One radiative channel can be achieved directly via electronic transitions from IMS III for PBN and IMS II for HBN to the valence band by the separation of the electron-hole pairs, which contributes to the higher frequency PL peak. Meanwhile, the electrons in IMS III for PBN and in IMS II for HBN can emit the LO-phonons and relax into further lowere IMESs and achieve radiative transition between these states and the valence band. The lower frequency PL peak is attributed to this process.

It is known that the IMESs induced by impurities and defects depend sensitively on the electronic band structure of the host semiconductor [39] and the band structure in a semiconductor can be affected strongly by the presence of the strain in the material [40, 41]. The presence of strain in a semiconductor can alter the dispersion relation and the symmetry of the electronic states and, as a result, can alter the energy levels and the symmetry of the IMESs. Together with the fact that PL from hBN is induced jointly by many-body electronic interactions such as phonon-assisted excitonic coupling and by electron-photon interactions among the IMESs, the different features of the PL and PLE spectra observed for PBN and HBN samples (such as the intensity, line-shape and peak position) can be excepted.

8. Conclusions

Motivated by the application of hBN based semiconductor as solid-state neutron detecting material, we have undertaken a detailed investigation into the influence of neutron irradiation on basic physical properties of PBN and HBN samples. The SEM and TEM have been applied for observation of the basic difference of the sample structures of PBN and HBN samples. The XRD and Raman spectroscopy have been used to examine the effect of neutron irradiation on out-plane and in-plane sample structures respectively. The PL measurements have been employed to study the effect of neutron irradiation on intermediate energy states induced by the presence of impurities

and defects in these samples. The main conclusions drawn from this study are summarized as follows.

The neutron irradiation does not alter the in-plane lattice structure in both samples. It has a very little effect on out-plane lattice structure of HBN samples but can release and easy the inter-layer tensions in PBN samples caused by the processes of sample growth. The neutron irradiation also affects very weakly the active IMES levels responsible for PL and PLE from both samples. However, the irradiation can reduce the effective carrier-phonon coupling, carrier-photon interaction and excitonic transitions in both samples. This is mainly due to the fact that the neutron irradiation can introduce the carrier trap centers in the sample. Overall, both PBN and HBN samples can have some degree of the resistance to neutron irradiation in terms of these basic physical properties. Interesting and surprisingly, we have found that two active IMES levels can result in one PL peak (which can be decomposed into two peaks) from PBN samples and one active IMES level can lead to two PL peaks from HBN samples. The energy spacing between two PL peaks is close to LO-phonon energy of hBN crystal.

The interesting and important findings from this work can benefit us to gain an in-depth understanding of the influence of neutron irradiation on basic physical properties of hBN materials. We believe that these effects can be helpful when designing and applying the hBN materials for neutron detectors.

Credit author statement. **Shun Zhou**: Data curation; Formal analysis, Roles Writing - original draft. **Wen Xu**: Supervision, Conceptualization, Writing-review&editing, Funding acquisition. **Yiming Xiao**: Data analysis. **Huan Xiao, Jing Zhang, Gaokui He, Jing Liu, Yuanyuan Li**: Methodology. **Zhu Wang**: Resources, Writing-review. **François M. Peeters**: Writing-review.

Declaration of competing interest. The authors declare that they have no known competing financial interests or personal relationships that could have appeared to influence the work reported in this paper.

Data availability. The data that support the findings of this study are available from the corresponding authors upon reasonable request.

References

1. R.T. Kouzes, J.H. Ely, L.E. Erikson, W.J. Kernan, A.T. Lintereur, E.R. Siciliano, D.L. Stephens, D.C. Stromswold, R.m. Van Ginhovern, M.L. Woodring, Neutron detection alternatives to 3He for national security applications, Nucl. Instrum. Meth. A 623 (2010) 1035-1045.

2. E. Aboud, S. Ahn, G.V. Rogachev, V.E. Johnson, J. Bishop, G. Christian, E. Koshchiy, C.E. Parker, D.P. Scriven, Modular next generation fast-neutron detector for portal monitoring, Nucl. Sci. Tech. 33 (2022) 13.

3. M.C. Hamel, J.K. Polack, M.L. Ruch, M.J. Marcath, S.D. Clarke, S.A. Pozzi, Active neutron and gamma-ray imaging of highly enriched uranium for treaty verification, Sci. Rep. 7 (2017) 7997.

4. G. Mauri, F. Messi, K. Kanaki, R. Hall-Wilton, F. Piscitelli, Fast neutron sensitivity for 3He detectors and comparison with Boron-10 based neutron detectors, Epj Tech. Instrum. 6 (2019) 3.

5. G.G. Fuentes, E. Borowiak-Palen, T. Pichler, X. Liu, A. Graff, G. Behr, R.J. Kalenczuk, M. Knupfer, J. Fink, Electronic structure of multiwall boron nitride nanotubes, Phys. Rev. B 67 (2003) 035429.

6. J.D. Caldwell, I. Aharonovich, G. Cassabois, J.H. Edgar, B. Gil, D.N. Basov, Photonics with hexagonal boron nitride, Nat. Rev. Mater 4 (2019) 552-567.

7. X.M. Duan, D.C. Jia, Z. Wang, D.L. Cai, Z. Tian, Z.H. Yang, P.G. He, S.J. Wang, Y. Zhou, Influence of hot-press sintering parameters on microstructures and mechanical properties of h-BN ceramics, J. Alloy. Compd. 684 (2016) 474-480.

8. G. Cappellini, G. Satta, Optical properties of BN in cubic and layered hexagonal phases, Phys. Rev. B 64 (2001) 035104.

9. A. Bommer, C. Becher, New insights into nonclassical light emission from defects in multi-layer hexagonal boron nitride, Nanophotonics-Berlin 8 (2019) 2041-2048.

10. J. Li, S. Majety, R. Dahal, W.P. Zhao, J.Y. Lin, Dielectric strength, optical absorption, and deep ultraviolet detectors of hexagonal boron nitride epilayers, Appl. Phys. Lett. 101 (2012) 171112.

11. F. Ferreira, A.J. Chaves, N.M.R. Peres, R.M. Ribeiro, Excitons in hexagonal boron nitride single-layer: a new platform for polaritonics in the ultraviolet, J. Opt. Soc. Am. B 36 (2019) 674-683.

12. K. Ahmed, R. Dahal, A. Weltz, J-Q. Lu, Y. Danon, I.B. Bhat, Growth of hexagonal boron nitride on (111) Si for deep UV photonics and thermal neutron detection, Appl. Phys. Lett. 109 (2016) 113501.

13. T.C. Doan, S. Majety, S. Grenadier, J. Li, J.Y. Lin, H.X. Jiang, Hexagonal boron nitride thin film thermal neutron detectors with high energy resolution of the reaction products, Nucl. Instrum. Meth. A 783 (2015) 121-127.

14. F. Ren, Y.Y. Wu, Z.W. Xu, Creation and repair of luminescence defects in hexagonal boron nitride by irradiation and annealing for optical neutron detection, J. Lumin. 261 (2023) 119911.

15. L. Liu, Y.P. Feng, Z.X. Shen, Structural and electronic properties of h-BN, Phys. Rev. B 68 (2003) 104102.

16. Q.H. Weng, X.B. Wang, X. Wang, Y. Bando, D. Golberg, Functionalized hexagonal boron nitride nanomaterials: emerging properties and applications, Chem. Soc. Rev. 45 (2016) 3989-4012.

17. F. Cataldo, S. Iglesias-Groth, Neutron damage of hexagonal boron nitride: h-BN, J. Radioanal Nucl. Chem. 313 (2017) 261-271.

18. J.H. Li, E.R. Glaser, C. Elias, G.H. Ye, D. Evans, L.J. Xue, S. Liu, G. Cassabois, B. Gil, P. Valvin, T. Pelini, A.L. Yeats, R. He, B. Liu, J.H. Edgar, Defect Engineering of Monoisotopic Hexagonal Boron Nitride Crystals via Neutron Transmutation Doping, Chem. Mater. 33 (2021) 9231-9239.

19. H. Zhang, M. Lan, G. Tang, F.L. Chen, Z.W. Shu, F.X. Chen, M. Li, Discrete color centers in two-dimensional hexagonal boron nitride induced by fast neutron irradiation, J. Mater. Chem. C 7 (2019) 12211.

20. B. Buyuk, Y. Goncu, A.B. Tugrul, N. Ay, Swelling on neutron induced hexagonal boron nitride and hexagonal boron nitride-titanium diboride composites, Vacuum 177 (2020) 109350.

21. A. Gügör, I.K. Akbay, T. Özdemir, EPDM Rubber with hexagonal Boron Nitride: A Thermal Neutron Shielding Composite, Radiation Phys. and Chem. 165 (2019) 1084391.

22. E.M. Huseynov, T.G. Naghiyev, N.R. Abbasov, The paramagnetic approach of the color-changing of nano h-BN particle under the neutron irradiation, Physica E 139 (2022) 115124.

23. D. Rafaja, V. Klemm, M. Motylenko, M.R. Schwarz, T. Barsukova, E. Kroke, D. Frost, L. Dubrovinsky, N. Dubrovinskaia, Synthesis, microstructure and hardness of bulk ultrahard BN nanocomposites, J. Mater. Res. 23 (2008) 981-993.

24. H.X. Jiang, J.Y. Lin, Review-Hexagonal Boron Nitride Epilayers: Growth, Optical Properties and Device Applications, ECS J. Solid State Sci. Technol. 6 (2017) Q3012.

25. I. Stenger, L. Schué, M. Boukhicha, B. Berini, B. Plaçais, A. Loiseau, Low frequency Raman spectroscopy of few-atomic-layer thick hBN crystals, 2D Mater. 4 (2017) 031003.

26. L. Museur, E. Feldbach, A. Kanaev, Defect-related photoluminescence of hexagonal boron nitride, Phys. Rev. B 78 (2008) 155204.

27. K. Ahmed, R. Dahal, A. Weltz, J.J-Q. Lu, Y. Danon, I. B. Bhat, Solid-state neutron detectors based on thickness scalable hexagonal boron nitride, Appl. Phys. Lett. 110 (2017) 023503.

28. T. Taniguchi, K. Watanabe, Synthesis of high-purity boron nitride single crystals under high pressure by using BaCBN solvent, J. Cryst. Growth 303 (2007) 525-529.

29. D.S. McGregor, T.C. Unruh, W.J. McNeil, Thermal neutron detection with pyrolytic boron nitride, Nucl. Instrum. Meth. A 591 (2008) 3.

30. B. Ertug, T. Boyraz, O. Addemir, Microstructural Aspects of the Hot-Pressed Hexagonal Boron Nitride Ceramics with Limited Content of Boron Oxide, Mater. Sci. Forum. 554 (2008) 197-200.

31. J. Koskelo, G. Fugallo, M. Hakala, M. Gatti, F. Sottile, P. Cudazzo, Excitons in van der Waals materials: From monolayer to bulk hexagonal boron nitride, Phys. Rev. B 95 (2017) 035125.

32. D.M. Hoffman, G.L. Doll, P.C. Eklund, Optical properties of pyrolytic boron nitride in the energy range 0.05-10 eV, Phys. Rev. B 30 (1984) 6051.

33. The results will be published elsewhere.

34. J.R. Toledo, D.B.de Jesus, M. Kianinia, A. S. Leal, C. Fantini, L.A. Cury, G.A.M. Sáfar, I. Aharonovich, K. Krambrock, Electron paramagnetic resonance signature of point defects in neutron-irradiated hexagonal boron nitride, Phys. Rev. B 98 (2018) 155203.

35. L. Museur, A. Kanaev, Photoluminescence properties of pyrolytic boron nitride, J. Mater. Sci. 44 (2009) 2560-2565.

36. Y.Z. Xue, H. Wang, Q.H. Tan, J. Zhang, T.J. Yu, K. Ding, D.S. Jiang, X.M. Dou, J-J. Shi, B-Q. Sun, Anomalous Pressure Characteristics of Defects in Hexagonal Boron Nitride Flakes, Acs Nano 12 (2018) 7127-7133.

37. G. Cassabois, P. Valvin, B. Gil, Hexagonal boron nitride is an indirect bandgap semiconductor. Nat. Photonics 10 (2016) 262−266.

38. S.J. Pearton, A. Aitkaliyeva, M. Xian, F. Ren, A. Khachatrian, A. Ildefonso, Z. Islam, M.A.J. Rasel, A. Haque, A.Y. Polyakov, J. Kim, ReviewRadiation Damage in Wide and Ultra-Wide Bandgap Semiconductors, ECS J. Solid State Sci. Technol. 10 (2021) 055008.

39. M. Maciaszek, L. Razinkovas, A. Alkauskas, Thermodynamics of carbon point defects in hexagonal boron nitride, Phys. Rev. Mater. 6 (2022) 014005.

40. L. Mennel, M.M. Furchi, S. Wachter, M. Paur, D.K. Polyushkin, T. Mueller, Optical imaging of strain in two-dimensional crystals, Nat. Commun. 9 (2018) 516.

41. C. Euaruksakul, Z.W. Li, F.J. Himpsel, C.S. Ritz, B. Tanto, D.E. Savage, X.S. Liu, M.G. Lagally, Influence of Strain on the Conduction Band Structure of Strained Silicon Nanomembranes, Phys. Rev. Lett. 101 (2008) 147403.